

Article

Trade-Off Curves for Performance Optimization in a Crushing Plant

Kanishk Bhadani ^{1,*}, Gauti Asbjörnsson ¹, Monica Soldinger Almfelt ², Erik Hulthén ¹
and Magnus Evertsson ¹

¹ Department of Industrial and Materials Science, Chalmers University of Technology, SE-412 96 Göteborg, Sweden; gauti@chalmers.se (G.A.); erik.hulthen@chalmers.se (E.H.); magnus.evertsson@chalmers.se (M.E.)

² Swerock AB, SE-401 80 Göteborg, Sweden; monica.almfelt@swerock.se

* Correspondence: kanishk@chalmers.se

Abstract: Operational flexibility in an aggregate production process is required to adapt to changes in customer demands. Excessive demand for a particular product fraction can lead to operational alteration wherein re-crushing of the existing larger-sized product fraction is necessary. The choice of re-crushing existing product fractions results in feed condition changes to the crusher. One common approach to producing the desired product is by varying the operation settings of a crusher in a crushing plant. However, knowledge of differences in operational performance for changing feed conditions in the circuit is required. This potentially leads to a problem of performance optimization based on the desired target product, available feed material and capability of the crusher. The paper presents an application of a multi-objective optimization method to generate multiple operational settings for the dynamic change in the operation condition in a crushing plant. Controlled experimental survey data with varying feed conditions are used to calibrate the crusher model using an unconstrained optimization problem solved using a gradient-based algorithm (Quasi-Newton method). Trade-off curves between various performance indicators of the crushing plant using a dynamic simulation platform are generated using multi-objective optimization using a non-gradient-based algorithm (genetic algorithm). The results of the application can help the operators and plant managers to make proactive decisions to steer the operation of the crushing plant towards the desired needs of the operation.

Keywords: optimization; dynamic simulation; comminution; Pareto-set; genetic algorithm; performance mapping; production balance; crusher calibration



Citation: Bhadani, K.; Asbjörnsson, G.; Soldinger Almfelt, M.; Hulthén, E.; Evertsson, M. Trade-Off Curves for Performance Optimization in a Crushing Plant. *Minerals* **2023**, *13*, 1242. <https://doi.org/10.3390/min13101242>

Academic Editor: Chiharu Tokoro

Received: 30 August 2023

Revised: 19 September 2023

Accepted: 22 September 2023

Published: 23 September 2023



Copyright: © 2023 by the authors. Licensee MDPI, Basel, Switzerland. This article is an open access article distributed under the terms and conditions of the Creative Commons Attribution (CC BY) license (<https://creativecommons.org/licenses/by/4.0/>).

1. Introduction

An aggregate production plant usually produces various sizes of rock products to meet different customer requirements. The products range from larger sizes, like 31.5 mm to 50 mm and 31.5 mm to 63 mm [1], used for railway ballast, to smaller sizes, such as 2 mm to 5 mm and 11 mm to 16 mm, used for making asphalt and concrete for road and building construction [2]. A typical scenario occurring in crushing plants in northern Europe is changing seasonal product demand from the market, for example, there is a higher demand for finer fractions (2/5 mm, 5/8 mm) in winter conditions compared to coarser products (11/16 mm, 16/22 mm), used in road networks for grip in iced road. There can be other localized changes in the product demands based on the geographic location of the crushing plant.

The crushing plant is equipped with a series of machines for crushing (e.g., jaw crusher and cone crusher), screening (e.g., vibratory screen), material transport (e.g., conveyors, loaders and feeder), and material storage (e.g., bin, silo and stockpile) to produce the different set of products. The plant design provides flexibility to control and drive production

towards the specific needs of the customer by controlling the settings of machines. For example, a cone crusher product can be controlled by changing CSS (closed-side setting), and adjusting the eccentric throw, and a vibratory screen product can be decided by altering screen panel type, sizes and settings. The experienced plant operator can understand certain relationships between these operating variables but as the plant complexity and operating variables grow, it becomes cognitively difficult to correlate the change to operational performance. Coupled with operational setting impacts, the dynamic process operation phenomenon (bin filling rate, material hold, material delays, etc.) also plays a role in plant product performance. Together with machine settings and dynamics, the operational decision becomes increasingly complex and difficult to interpret [3,4]. To facilitate decision making for complex relationships, dynamic process simulation tools need to provide functionality for operators to make optimization decisions.

Figure 1 shows a modular framework consisting of multiple layers of development needed for the implementation of optimization capability for crushing plants [5]. Developing a reliable and suitable functionality for decision making in crushing and screening processes using a simulation platform requires multiple methodical developments. The essence of the proposed framework is to increase the performance control of the crushing plant by utilizing simulation systems with suitable functionality.

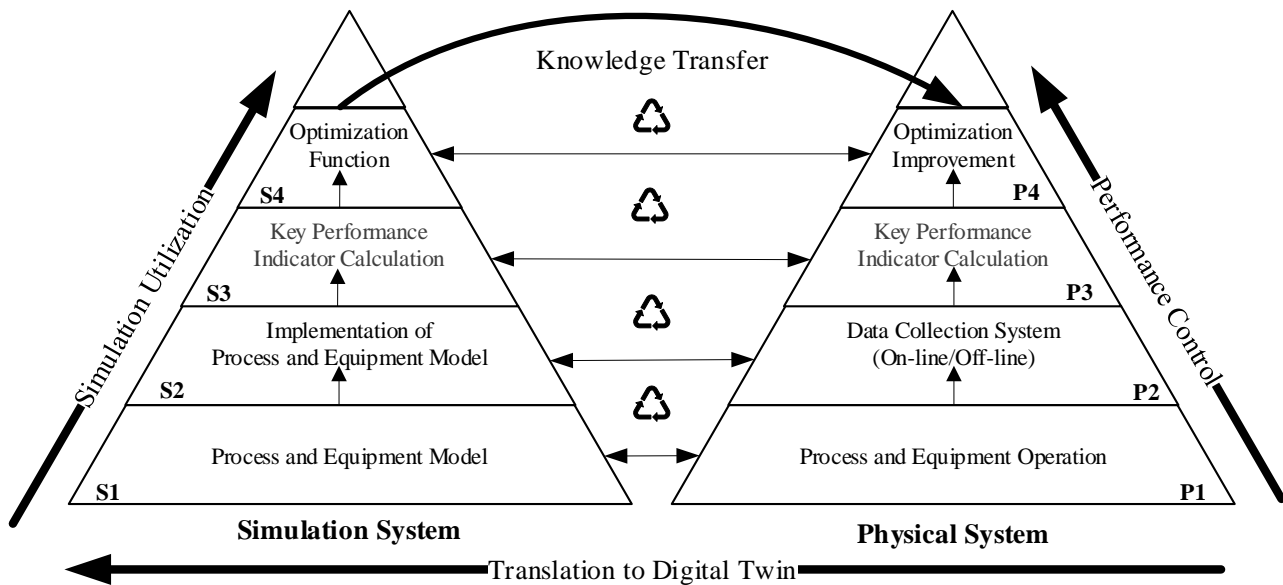


Figure 1. A modular framework for the implementation of optimization capabilities for crushing plants [5].

There is a wide range of models available to replicate the functionality of the physical equipment [6,7]. The model of cone crusher and screens can be described based on mechanistic principles [8,9], phenomenological principles [10] and empirical principles [7,11,12]. These models help in designing new crushing plants but are limited in providing functionality for daily operations. To make decisions for daily operation, the reliability of the model output becomes a necessary requirement [13,14]. Another aspect to consider is finding suitable performance indicators that can help operators make daily operational decisions [15,16]. The performance indicators need to be interpretable for decision-making. Lastly, the functionality of optimization needs to be supporting the interpretation of the performance indicators [17]. Previous research has shown partial implementation of methods, for example, the calibration/validation of the process/equipment model [14,18], and the optimization of the process plant [17,19–21] and is limited to a holistic application covering the bottom-up approach as shown in Figure 1.

In this research paper, an optimization case study for an industrial crushing plant producing multiple aggregate products is presented. The systematic implementation of

multiple optimization methods within the simulation system (S1–S4) is demonstrated. Two types of optimization methods are applied in this research work. Firstly, a computationally efficient unconstrained gradient-based approach (Quasi-Newton method) is used to calibrate the crusher model. This is followed by the configuration of the dynamic process simulation model in MATLAB/Simulink for mapping the industrial test site. Secondly, a non-gradient-based optimization method (multi-objective genetic algorithm) is used to generate a trade-off (Pareto-front) using the response from the dynamic process simulation. Specifically, three key performance indicators (KPIs) relevant to the site are used for trade-off curves: product throughput, product quantity and product yield [15].

2. Industrial Crushing Plant Site

The aggregate production site used in the research consists of tertiary and quaternary stages (See Figure 2) of a larger production facility situated in West Sweden. This segment of the facility is built with the flexibility to either produce large quantities of railway ballast (P1) or smaller fractions of products (P2–P7) used for road and building constructions (controlled by splitter T0).

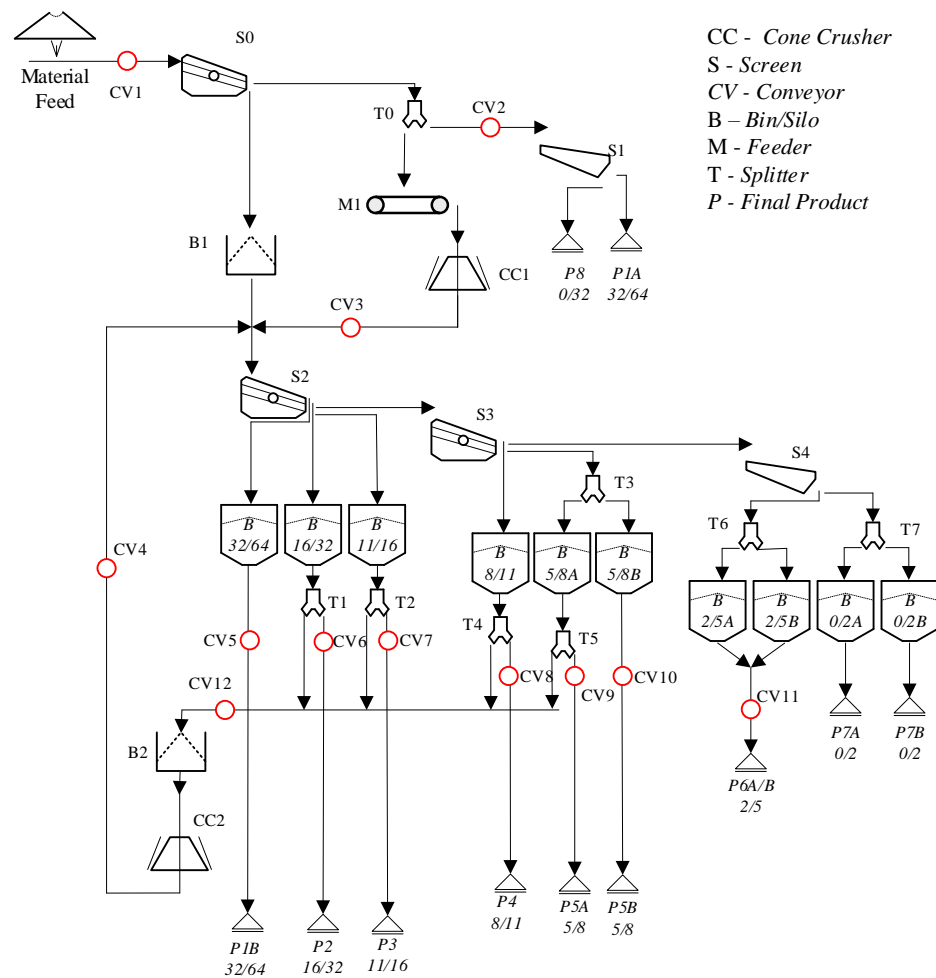


Figure 2. Section of the crushing plant site at Källered Bergtäkt, Swerock, Sweden.

Out of the two situations, this study focuses on configuration wherein the production of products P2–P7 needs balancing. The throughput of products (P2–P7) is dependent on the configuration of the tertiary crusher (CC1—H3000) and quaternary crusher (CC2—H36). The crusher CC1 is operated with a fixed feed PSD from screen S0 while the crusher CC2 is operated with varying feed PSD depending on the operators’ decision of the re-crushing products (P2, P3, P4 and P5). There are external conditions which govern these decisions such as customer demands, the status of stockpile level and the filling rate of the product

storage silos. Each selected feed PSD to CC2 creates a configuration scenario for the crushing plant. Due to varying production rates, the bin/silo filling rate of various products (P2–P5) differs which leads to dynamic operational situations where bottlenecks can occur. This results in a need to re-crush products if the backup stockpiles have reached the target capacity or if the silo has reached its capacity limit. There are two optimization situations which can occur in such complex operations:

1. For a given configuration scenario of plant operation and selected re-crushing product stream, what is the trade-off possible in the production KPIs of different product streams?
2. What is the appropriate set of configuration scenarios operation possible to reach a target customer need from the production facility (considering the dynamic nature of the production, time duration and crusher setting)?

This research will particularly focus on question 1, wherein trade-off curves for different operational configurations will be explored for various KPIs of the plant performance.

3. Method Description

The method applied is divided into three parts: Modeling and Simulation Methods, Experimental Methods and Optimization Methods. A brief account of different applied techniques is presented in this section.

3.1. Modeling and Simulation Method

A systematic approach is applied to configure a two-stage industrial crushing plant in the MATLAB/Simulink environment. The dynamic simulation approach as demonstrated by Asbjörnsson [3] is applied process modeling of the crushing plant. The simulation can capture operational behaviors, for example, material delay, start-stop sequences of equipment, discrete events, control loops, etc. [3,13,22]. The mathematical equations used for representing mass m and properties γ with respect to time at a given node in the circuit are given by Equations (1) and (2) [3].

$$\frac{dm(t)}{dt} = (\dot{m}_{i,in}(t) - \dot{m}_{j,out}(t)) \quad (1)$$

$$\frac{d\gamma(t)}{dt} = \frac{\dot{m}_{i,in}(t)}{m(t)} (\gamma_{i,in}(t) - \gamma(t)), \text{ where } \gamma(t) = \begin{bmatrix} \gamma_1(t) \\ \vdots \\ \gamma_n(t) \end{bmatrix} \quad (2)$$

The crusher model used in the application is a simplified Whiten's Cone Crusher model (see Equation (3)), where p is the product stream, f is the feed stream, C is the classification function, B is the breakage function and I is an identity matrix [7].

$$p = (I - C) * (I - BC)^{-1} * f \quad (3)$$

The classification function C is given by the probability function shown in Equation (4), where K_1 to K_3 are dependent on cone crusher parameters and xs_i is the sieve size class. The model is used as an empirical approach to mapping the cone crusher performance, the parameters K_1 and K_2 were simplified to be only dependent on the closed-side setting (CSS) and throughput (MF) of the tested crushers while K_3 is treated as an independent variable [7].

$$C_i = \begin{cases} 0, & \text{for } xs_i \leq K_1 \\ 1 - \left(\frac{K_2 - xs_i}{K_2 - K_1} \right)^{K_3} & \text{for } K_1 < xs_i < K_2 \\ 1, & \text{for } xs_i \geq K_2 \end{cases} \quad (4)$$

$$K_1 = a_0 + a_1 CSS - a_2 MF$$

$$K_2 = b_0 + b_1 CSS + b_2 MF$$

$$K_3 = c_0$$

The breakage function B used is based on the Reid–Stewart form, see Equation (5), where ϕ , λ and β are calibratable factors depending on the material characterization [23].

$$B_{ij} = \phi \left(\frac{x_{s_i}}{x_{s_j}} \right)^\lambda + (1 - \phi) \left(\frac{x_{s_i}}{x_{s_j}} \right)^\beta \quad (5)$$

The mass flow of the crusher is modeled using the geometric dimension and CSS value of the crusher and is calibratable using a parameter alpha (α) [24]. The power draw of the crusher is estimated using the Bond equation [25]. The total calibratable variables for the crusher model are given by the vector in Equation (6).

$$\mathbf{x}_k = [a_0, a_1, a_2, b_0, b_1, b_2, c_0, \phi, \lambda, \beta, \alpha] \quad (6)$$

The screen model is based on the Whiten expression as shown in Equation (7), where E_{oa} represents the reduced partition curve for calculating the oversized material stream, α is the sharpness of the separation, d_i is the geometric mean of the size interval i in sieve size class x_{s_i} , d_{50} is the separation size, E is the efficiency at the screen aperture and A is the screen aperture [7,14].

$$\begin{aligned} E_{oa} &= \frac{\exp(\alpha x_i) - 1}{\exp(\alpha x_i) + \exp(\alpha) - 2} \\ x_i &= \frac{d_i}{d_{50}} \\ d_{50} &= \frac{\alpha A}{\ln\left[\left(\frac{100}{100-E} - 1\right) \exp(\alpha) + \left(\frac{100}{100-E} - 1\right) - 2\right]} \end{aligned} \quad (7)$$

Bins, splitters and stockpiles are modeled using the perfect-mix principle and first-in-first-out (FIFO) principle [3,26]. Conveyors are modelled using the state-space model and represent material delay units in the dynamic process simulation [3]. Power estimations are based on the mechanistic model principle and are based on a simple linear model using mass flow value [3]. The material flow between crushers, bins and conveyors is regulated using interlocks and controlled using a PI controller [3].

3.2. Experimental Method

An experimental method was applied to map the performance of the two crushers (CC1 and CC2). The purpose of the experiment is to map the input to the crusher such as feed PSD and CSS to crusher output such as mass flow, power, pressure and product PSD. Table 1 shows the experimental plan and recorded values for crusher CC1. The crusher was calibrated using an inbuilt function of mantle-to-mantle calibration. For this study, four settings of CSS were tested for a constant feed PSD. For each test, the crusher was operated to achieve a stable power signal followed by a crash stop sequence. Adequate representative samples of belt-cut samples were collected for each test based on the top size of the particle and sieving standard [7,27]. Sieving analysis was performed on each sampled material using the SS-EN 933-1:2012 standard [27].

Table 2 shows the experimental plan and recorded values for crusher CC2. The crusher was calibrated using the inbuilt function of mantle-to-mantle calibration. For this study, three settings of CSS were tested for three different feed PSDs. For each test, the crusher was operated to achieve a stable power signal followed by a crash stop sequence. Adequate representative samples using belt-cut were collected for each test and sieving analysis was performed on each sampled material using SS-EN 933-1:2012 standard [27]. The operation of the crusher and setting change was critical in this experiment as the different feed type creates different packing density inside the crusher chambers. The minimum CSS operation of the crusher was limited by the safety pressure setting in the control system. A low CSS value was selected for the first run for each feed type to push the crusher at the maximum pressure setting. The purpose of performing three samples for each feed was to eliminate the risk of sampling errors with crusher operation.

Table 1. Experimental plan and noted values for the crusher CC1 in the crushing plant.

Test ID	CSS Setpoint [mm]	ASRi CSS [mm]	Pressure [MPa]	Power [kW]	Belt-Cut Sampling Point
C01	CSS Calibration	-	-	-	-
T01	20	20.6	5.90	130	Feed and Product
T02	22	21.8–22.2	3.8	103	Product
T03	24	24	4.1	99	Product
T04	26	26	3.3	90	Product

Table 2. Experimental plan and noted values for the crusher CC2 in the crushing plant.

Test ID	Feed	CSS Setpoint [mm]	ASRi CSS [mm]	Pressure [MPa]	Power [kW]	Belt-Cut Sampling Point
C11	-	CSS Calibration	-	-	-	-
T11	Feed 1 P3–11/16	5	7.1	3.5	45	Feed and Product
T12	Feed 1 P3–11/16	7	7.2	3.3	44	Product
T13	Feed 1 P3–11/16	10	10.3	1.8	30	Product
C12		CSS Calibration	-	-	-	-
T14	Feed 2 P4–8/11	5	7	3.5	42	Feed and Product
T15	Feed 2 P4–8/11	8	8.4	2.6	35	Product
T16	Feed 2 P4–8/11	10	10.3	1.7	25	Product
C13	-	CSS Calibration	-	-	-	-
T17	Feed 3 P5–5/8	4	7.1	3.5	40	Feed and Product
T18	Feed 3 P5–5/8	8	8.3	2.6	31	Product
T19	Feed 3 P5–5/8	10	10.3	1.6	21	Product

The screens were not sampled as it was in an inaccessible location at the site. The screen is assumed to be performing in an ideal condition of operation. The screen model was configured with standard operational value for efficiency ($E = 95$) and sharpness ($\alpha = 13$) factor while the aperture was tuned based on the site data.

3.3. Optimization Method

Two distinct applications of optimization methods are used in this research: Optimization for Crusher Model Calibration and Optimization for Trade-off Analysis using Key Performance Indicators.

3.3.1. Optimization for Crusher Model Calibration

The crusher model is calibrated based on the survey sampling performed at the industrial site. All the crusher model parameters were backfitted using an unconstrained gradient-based optimization algorithm, the Quasi-Newton method [14,28]. The crusher model is treated as completely empirical based on the data from belt-cut experiments. The crusher model was sequentially calibrated for capacity and product size distribution, see Equations (8) and (9). A similar optimization approach has been previously demonstrated in the fast mechanistic crusher model based on the Evertsson crusher model [8,14].

Capacity Optimization: The objective function is to minimize the sum of the relative errors between crusher measured capacity (Cap_{Di}) to simulated capacity (Cap_{Si}) for the n number of tested settings of CSS.

$$\min \sum_{i=1}^n \left| \frac{Cap_{Di} - Cap_{Si}}{Cap_{Di}} \right|$$

$$w.r.t \rightarrow x_k, [k = 11]$$

$$Optimizer = x_k^*$$
(8)

PSD Optimization: The objective function is to minimize the weighted (w_j) sum of errors for the data ($PSDf_{Dji}$) and the simulation ($PSDf_{Sji}$) for the values of the n number of tested settings. The PSD values are in the frequency domain for m number of given sieve sizes (x_{si}). The weighted function (w_j) is given in Equation (10), which is a function of the sieve size used in the simulation for weighing the data points within a sieve size range. The PSD in the frequency and the cumulative domain is in fraction passing for the sieve size.

$$\min \sum_{i=1}^n \sum_{j=1}^m w_j |(PSDf_{Dji} - PSDf_{Sji})|$$

$$w.r.t \rightarrow x_k, [k = 1, 2, \dots, 10]$$

$$Optimizer = x_k^*$$
(9)

$$z_j = \log_2(xsize_j) + |\log_2(\min(\mathbf{xsize}))|$$

$$w_j = \begin{cases} z_j / (\max(\mathbf{z})) \forall (j = 1, 2, \dots, 24) \\ 1, (j = 25) \end{cases}$$
(10)

where,

$$\mathbf{xsize} = [360; 250; 125; 90; 63; 45; 31.5; 22.4; 16; 11.2; 8; 5.6; 4; 2.8; 2; 1.4; 1; 0.7; 0.5; 0.35; 0.25; 0.177; 0.125; 0.088; 0.063]$$

3.3.2. Optimization for Trade-Off Analysis Using Key Performance Indicators

Multi-objective optimization (MOO) is used to generate a trade-off analysis (Pareto Front) between competing objective functions in each problem definition [29–31]. A generic optimization problem definition for two competing objective functions (f_1, f_2) and a set of constraints (\mathbf{c}) is shown in Figure 3 [5]. Here, a genetic algorithm is applied to solve a MOO problem [32]. For the current application the design variables (\mathbf{x}) are represented by the operational setting of crushers (CSS1 and CSS2) while the output variables (\mathbf{y}) are performance values of mass flow, power, etc. Using the different performance values from simulation, objective functions can be formulated such as product throughput rate, product yield, product quantity and specific energy [15]. The approach treats the entire crushing plant as one system and the algorithm iteratively communicates with the simulation to explore the design space of the problem.

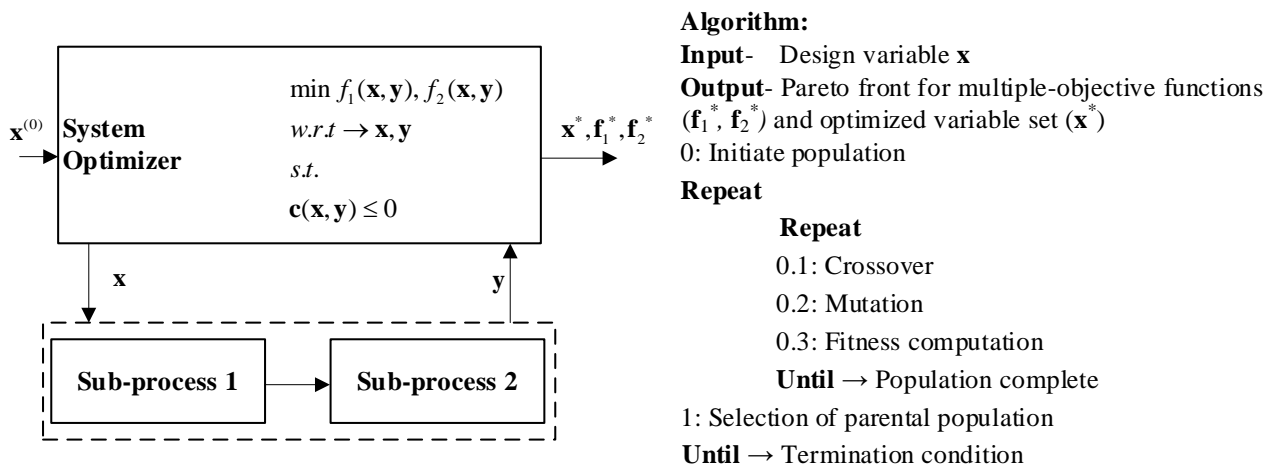


Figure 3. Optimization problem formulation and algorithm for the MOO problem using genetic algorithm [5].

4. Results

The results section is divided into three parts: crusher calibration, process configuration result and trade-off curves for KPIs.

4.1. Crusher Calibration Results

The crusher calibration is based on the back fitting of the crusher model with the belt-cut data. Figure 4a,b present the crusher calibration results for different tested CSS in the cumulative domain and frequency domain, respectively, for the optimization problem posed for crusher CC1 (refer to Equation (7)).

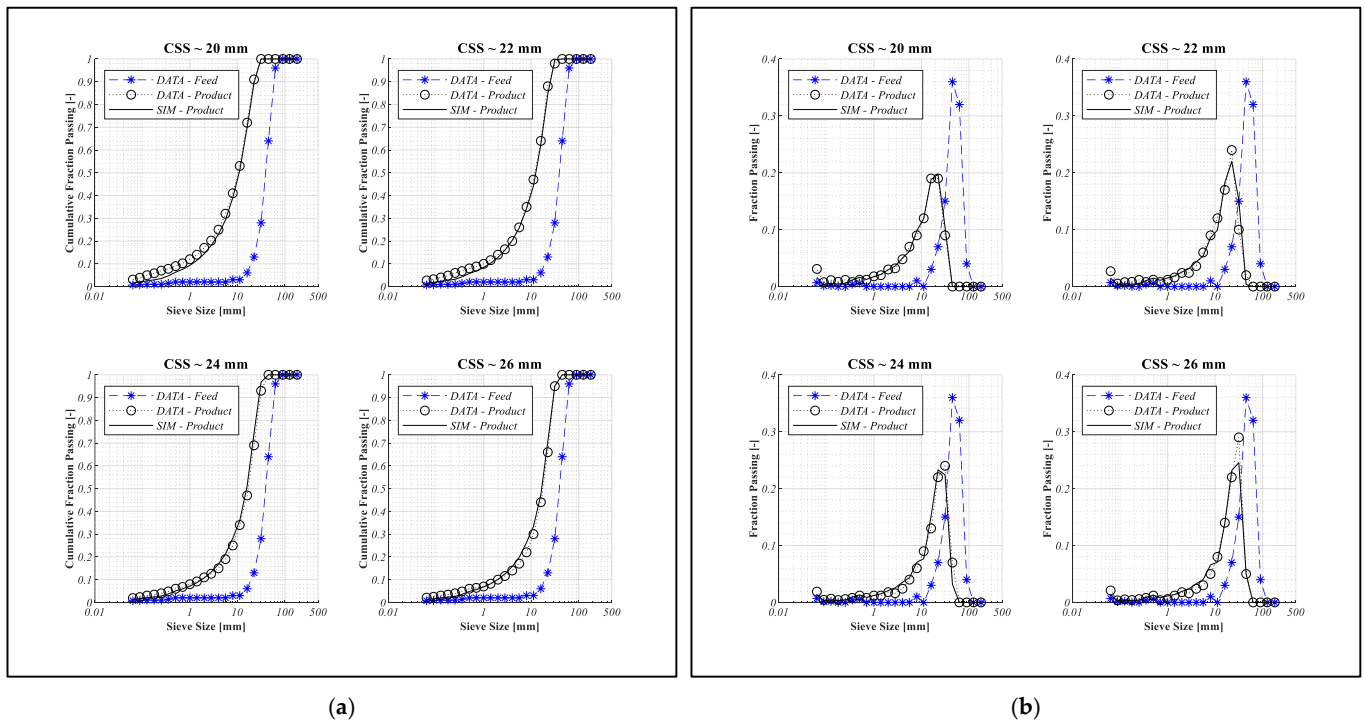


Figure 4. Cone crusher CC1 calibration to the belt-cut data in (a) cumulative domain and (b) frequency domain for varying feed and CSS.

Figure 5a,b present the crusher calibration results for different tested feeds and CSS in the cumulative domain and frequency domain, respectively, for the optimization problem posed by crusher CC2 (refer to Equation (7)). For the crusher CC2, three experiments were carried out for each feed condition although the optimization was performed with two selected experimental data for each feed condition. This was used to avoid overfitting the model and also to reject the outlier or corrupted datasets. Both the crusher calibration results show good conformance with the data gathered from the experiment. Also, the application of the Quasi-Newton method was found to be computationally efficient which is in line with previous applications [14].

Figure 6 shows the calibrated capacity of the two crushers with respect to the CSS change. Table 3 presents the optimized variables for the empirically fitted model for both cone crusher CC1 and CC2. Since the model is empirically fitted using belt-cut samples without material characterization tests, the interpretation of the calibrated coefficients is limited. Compared to the constrained optimization problem for crusher model calibration [18], the presented unconstrained optimization problem formulation is a simplified approach with less number of variables. The strategy of calibration is a two-step process with capacity calibration followed by PSD calibration.

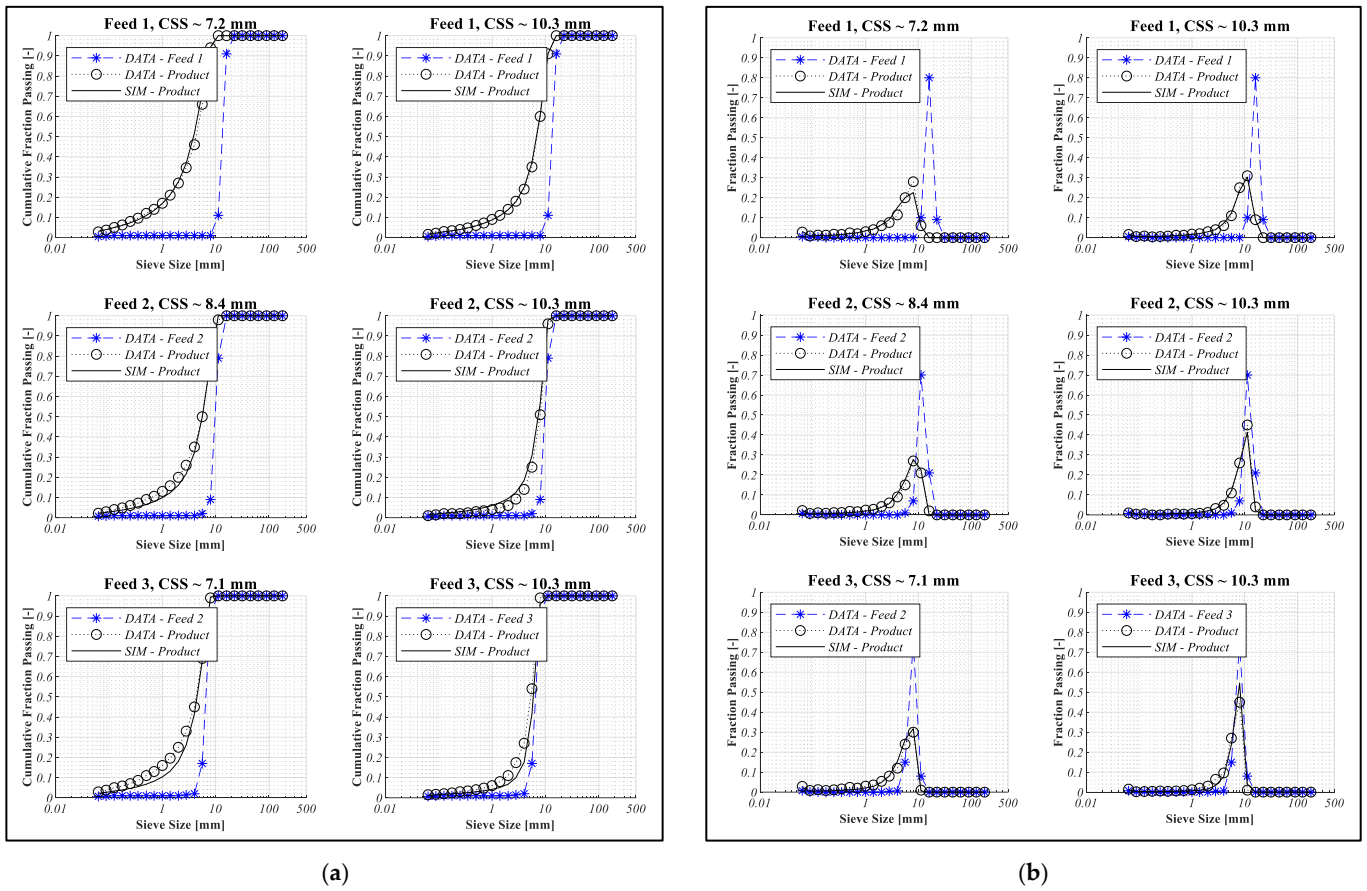


Figure 5. Cone crusher CC2 calibration to the belt-cut data in (a) cumulative domain and (b) frequency domain for varying feed and CSS.

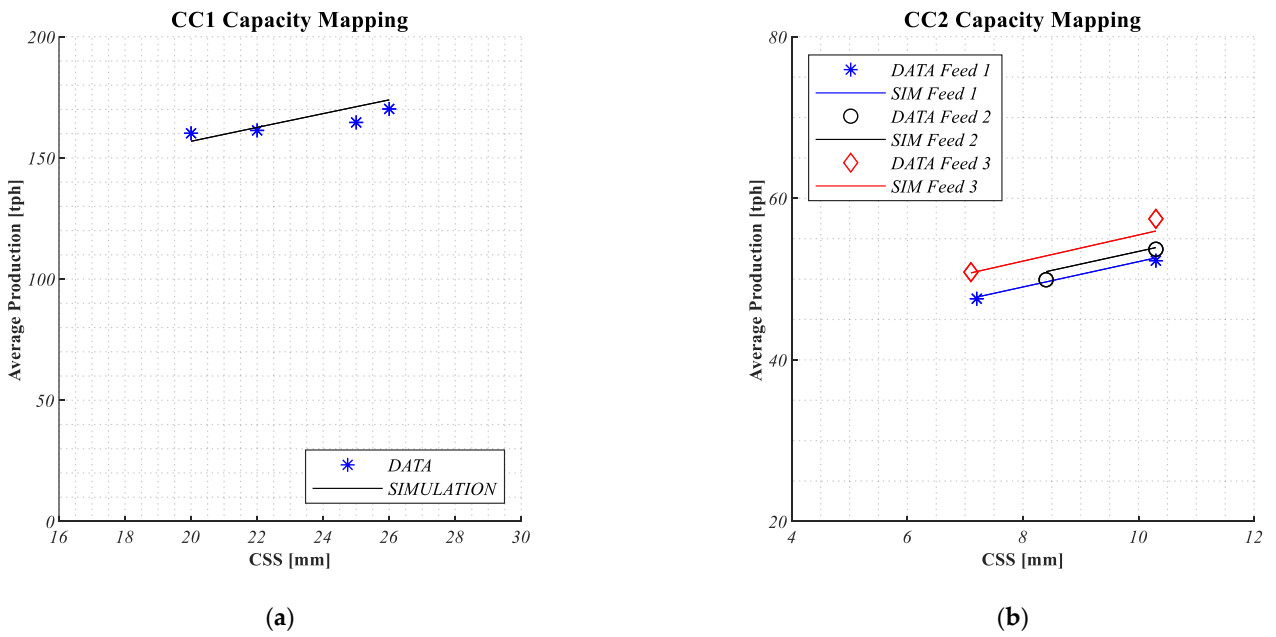


Figure 6. Capacity mapping of cone crusher (a) CC1 and (b) CC2.

Table 3. Fitted parameters of the cone crusher model.

Cone Crusher	a_0	a_1	a_2	b_0	b_1	b_2	c_0	φ	λ	β	α
CC1	0.0036	2.1882	0.7518	−0.0091	0.8587	0.6353	2.3424	0.3371	0.76144	5.0079	0.830
CC2	−0.1246	1.8353	1.4846	−0.1597	1.583	0.0777	1.3013	0.08194	0.6876	4.6074	0.595, F1 0.600, F2 0.610, F3

4.2. Dynamic Process Simulation Results

The crushing plant was configured in a Simulink environment, see Figure 7. In this instance of simulation configuration, the product stream P3–11/16 is recirculated back for re-crushing in crusher CC2. The flow of material from the bin before the cone crusher CC2 is controlled based on the level setpoints. The materials start flowing when the level reaches 90% of the bin capacity and stop when the bin level reaches a lower limit of 10%. The mass flow rate for different products for a setting at CSS1 = 20 mm and CSS2 = 6 mm is shown in Figure 8 and CSS1 = 26 mm and CSS2 = 10 mm is shown in Figure 9. By changing the CSS points, the production rate of different products changes affecting the bin filling rate and causing different times of on and off operation of crusher CC2. Also, the total amount of product produced can be obtained by integrating the area under different product mass flows.

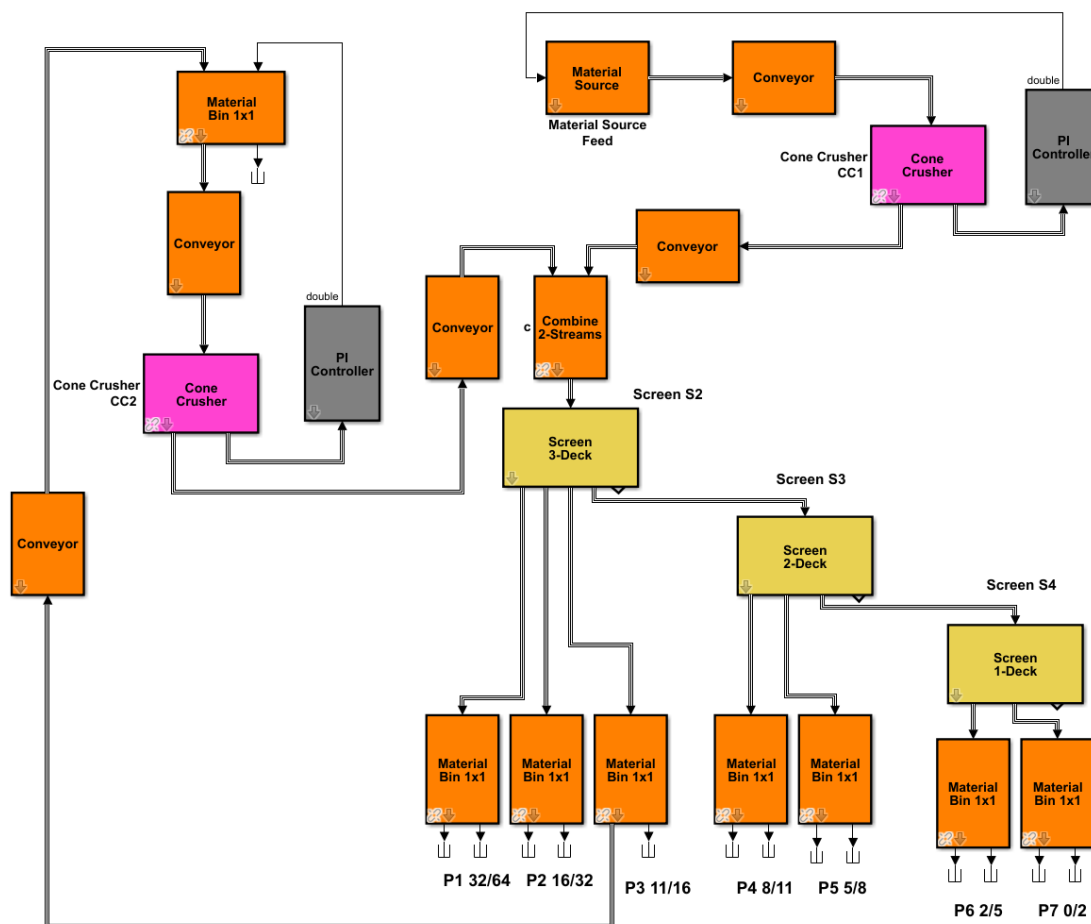


Figure 7. Dynamic process simulation configuration in Simulink environment.

As observed in Figures 8 and 9, there is a wide range of operational production rates as the two crusher settings are changed. It can also be observed that the change in magnitude of the mass flow rate is different depending on the product specification. This implies that the optimization problem solution will vary depending on what product is posed in the

objective of the problem as there is the underlying varying sensitiveness of each product based on the closed-side setting of the crusher, coupled with the topology of the plant.

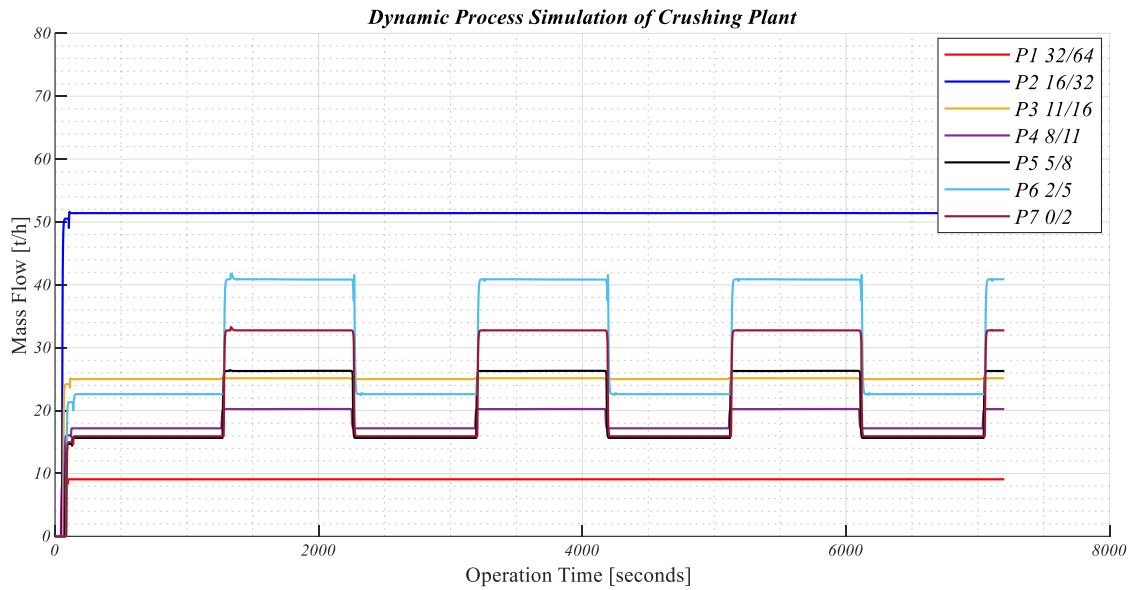


Figure 8. Mass flow rates of different products for one instance of simulation configuration: CSS1 = 20 mm and CSS2 = 6 mm.

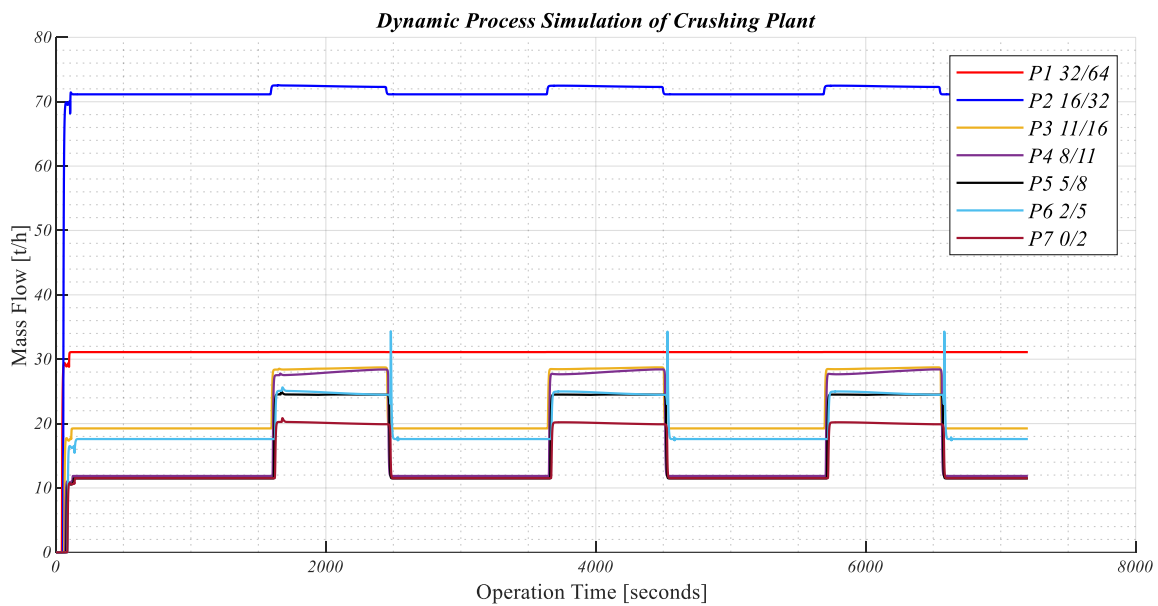


Figure 9. Mass flow rate of different products for one instance of simulation configuration: CSS1 = 26 mm and CSS2 = 10 mm.

4.3. Trade-Off Analysis of Production KPIs

The application of trade-off analysis is usually applied for competing objective functions. The objective functions formulated for trade-off contain either one product or a combination of products that can help in process performance exploration and decision-making. The key performance indicators for different final products of interest here are:

- **Throughput Rate (TR)**—The value of the mass flow rate of different product streams. In this application, the throughput rate is retrieved when both crusher CC1 and CC2 are operating.

- Product Quantity (Q)—The quantity of each product produced for a given operation time. It is given by the integration of the throughput rate with respect to the operation time.
- Product Yield (PY)—The proportion of each product compared to the total sum of different products produced for a given time of operation. This can be obtained either using throughput rate or product quantity functions.

Case 1: The trade-off curves are generated for an operational scenario where the product P11/16 is recirculated for re-crushing. Figure 10a shows the trade-off curve generated for two objective functions f_1 and f_2 expressed as production quantity in tons, as shown in Equation (11). The respective solution points are shown in Figure 10b. It can be observed that the major production change happens as CSS1 is reduced. There is an almost linear decrease in the production of f_2 and a corresponding increase in f_1 between solution points 3 and 11. After this point, the change in f_2 is minimal and the value of function f_1 is increased by reducing the CSS2 setting. This example shows the different sensitivities of the variables CSS1 and CSS2 on the production quantity of the two functions coupled with the effect of the choice of re-crushing material. Sensitivities mean a change in the magnitude of a variable brings different changes in output function.

$$\begin{aligned}
 &\min f_1 = P5/8Q + P2/5Q, f_2 = P16/32Q \\
 &w.r.t \rightarrow CSS_1, CSS_2 \\
 &s.t. \\
 &20 \leq CSS_1 \leq 26 \\
 &6 \leq CSS_2 \leq 10 \\
 &where, f_1 \text{ and } f_2 \text{ is expressed as [t]}
 \end{aligned}
 \tag{11}$$

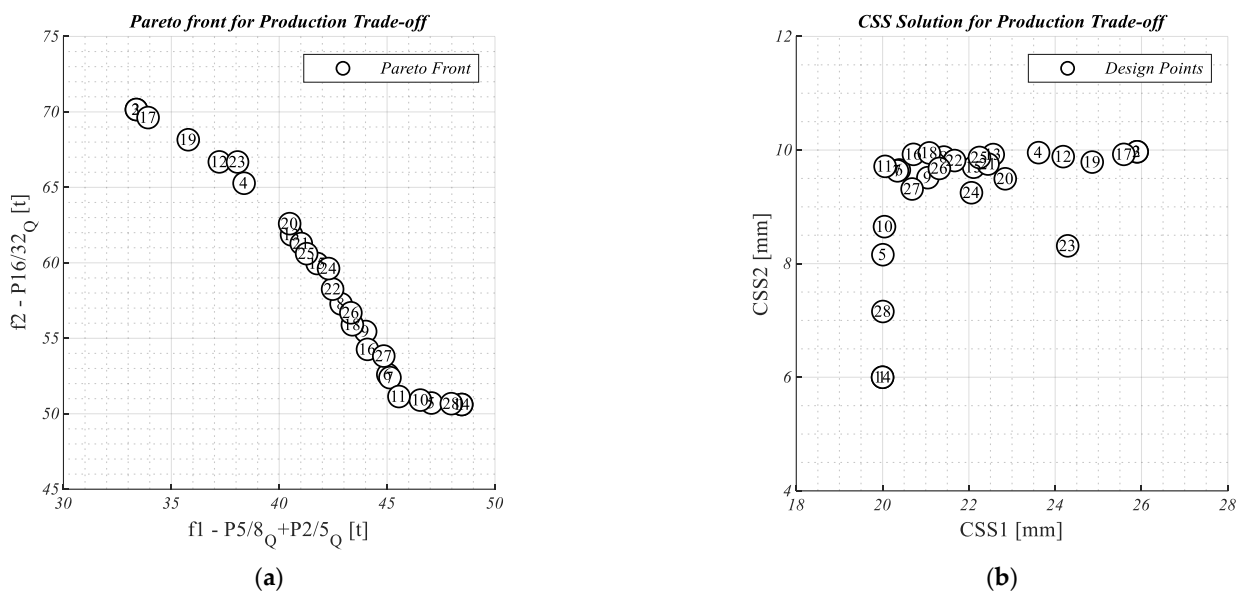


Figure 10. (a) Trade-off curve and (b) solution points of the optimization problem in Equation (11), when P11/16 is recirculated.

Case 2: The trade-off curves are generated for an operational scenario where the product P8/11 is recirculated for re-crushing. Figure 11a shows the trade-off curve generated for two objective functions f_1 and f_2 expressed as mass flow rate under the condition of both crushers is in an operational state, as shown in Equation (12). The respective solution points are shown in Figure 11b. The trend in results of the trade-off curve is similar to case 1, although, the magnitude of objective functions and the solution space are completely different. The solutions space for optimizer CSS2 is interior optima as compared to the boundary optima in Case 1. This example shows the different results of the objective

function in the solution space in comparison with Case 1 coupled with the effect of change in the recirculating load.

$$\begin{aligned}
 &\min f_1 = P2/5_{TR} + P11/16_{TR}, f_2 = P16/32_{TR} \\
 &w.r.t \rightarrow CSS_1, CSS_2 \\
 &s.t. \\
 &20 \leq CSS_1 \leq 26 \\
 &6 \leq CSS_2 \leq 10 \\
 &where, f_1 \text{ and } f_2 \text{ is expressed as [t/h]}
 \end{aligned}
 \tag{12}$$

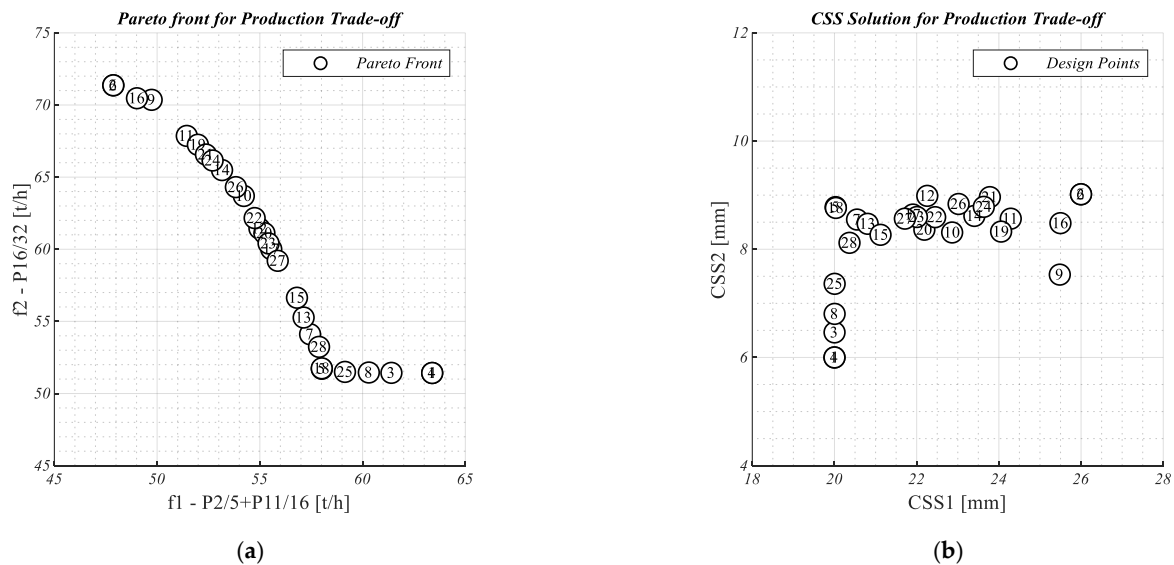


Figure 11. (a) Trade-off curve and (b) solution points of the optimization problem in Equation (12), when P8/11 is recirculated.

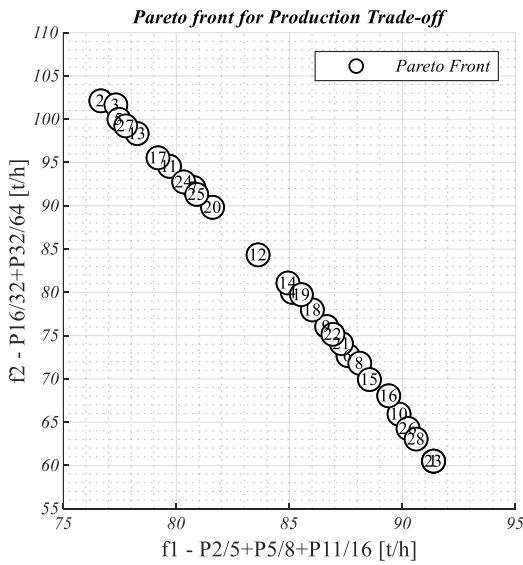
Case 3: This case is an extension of case 2, where the trade-off curves are generated for an optimization problem with the extension of two objective functions f_1 and f_2 to include more products, as shown in Equation (13). The operational scenario is with the re-crushing of the product P8/11. Figure 12a shows the trade-off curve generated for two objective functions f_1 and f_2 and Figure 12b shows the respective solution points. The trend in the results of the trade-off curve is linear between the two functions. The solutions space for optimizer CSS2 is lying on the lower bound value in comparison with cases 1 and 2. This example shows the effect of the objective function made with a higher number of individual products coupled with the grouping of products in the objective.

$$\begin{aligned}
 &\min f_1 = P2/5_{TR} + P5/8_{TR} + P11/16_{TR}, f_2 = P16/32_{TR} + P32/64_{TR} \\
 &w.r.t \rightarrow CSS_1, CSS_2 \\
 &s.t. \\
 &20 \leq CSS_1 \leq 26 \\
 &6 \leq CSS_2 \leq 10 \\
 &where, f_1 \text{ and } f_2 \text{ is expressed as [t/h]}
 \end{aligned}
 \tag{13}$$

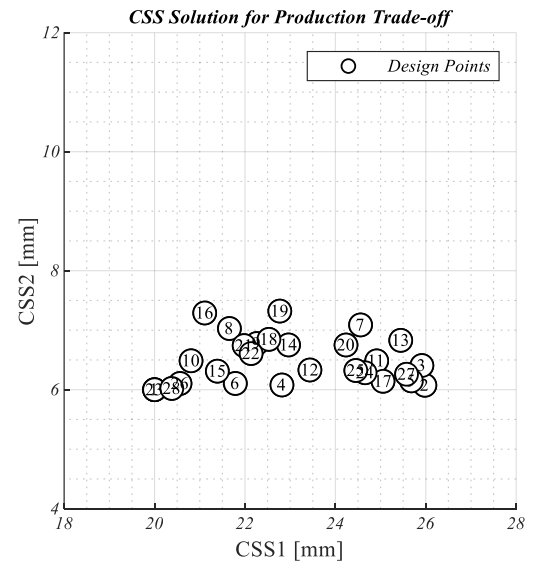
Case 4: For the re-crushing of product P11/16, the trade-off curve for objective function as the product yield (calculated using throughput rate) is generated. Equation (14) shows the optimization problem definition which is similar to Case 1 objective functions. Figure 13a) shows the trade-off curve expressed as per cent between the two objectives and Figure 13b) shows the respective solution point. As interpreted by the trade-off curve, the yield can be controlled between the two objectives in a range of 8% to 15% which represents the flexibility region available in processing. Also, the solution space is found to be in the boundary region indicating the decoupling of the objectives based on the circuit topology.

This example shows the sensitivities of the variables CSS1 and CSS2 on the product yield of the two functions for a given re-crushing product.

$$\begin{aligned}
 &\min f_1 = PY5/8_{TR} + PY2/5_{TR}, f_2 = PY16/32_{TR} \\
 &w.r.t \rightarrow CSS_1, CSS_2 \\
 &s.t. \\
 &20 \leq CSS_1 \leq 26 \\
 &6 \leq CSS_2 \leq 10 \\
 &where, f_1 \text{ and } f_2 \text{ is expressed as } [\%]
 \end{aligned}
 \tag{14}$$

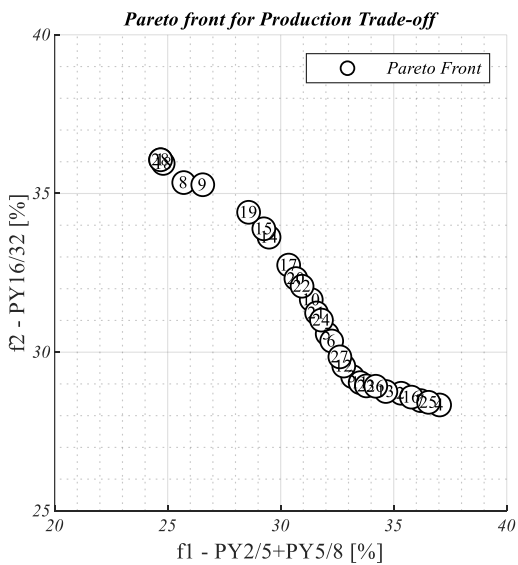


(a)

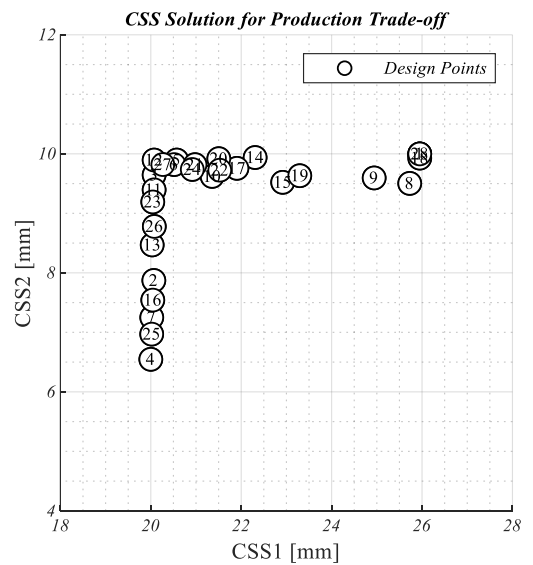


(b)

Figure 12. (a) Trade-off curve and (b) solution points of the optimization problem in Equation (13), when P8/11 is recirculated.



(a)



(b)

Figure 13. (a) Trade-off curve and (b) solution points of the optimization problem in Equation (14), when P11/16 is recirculated.

Case 5: For the re-crushing of product P8/11, the trade-off curve for objective function as product yield (calculated using throughput rate) is generated. Equation (15) shows the optimization problem definition which is similar to Case 2 objective functions. Figure 14a shows the trade-off and Figure 14b shows the respective solution point. The solution points are interior optima for both CSS1 and CSS2. The product yield function is suitable for operational situations when the objective is to minimize/maximize the proportion of a certain product range. This example shows the sensitivities of the variables CSS1 and CSS2 on the product yield of the two functions coupled with a change in recirculating load.

$$\begin{aligned}
 &\min f_1 = PY5/8_{TR} + PY11/16_{TR}, f_2 = PY16/32_{TR} \\
 &w.r.t \rightarrow CSS_1, CSS_2 \\
 &s.t. \\
 &20 \leq CSS_1 \leq 26 \\
 &6 \leq CSS_2 \leq 10 \\
 &where, f_1 \text{ and } f_2 \text{ is expressed as } [\%]
 \end{aligned}
 \tag{15}$$

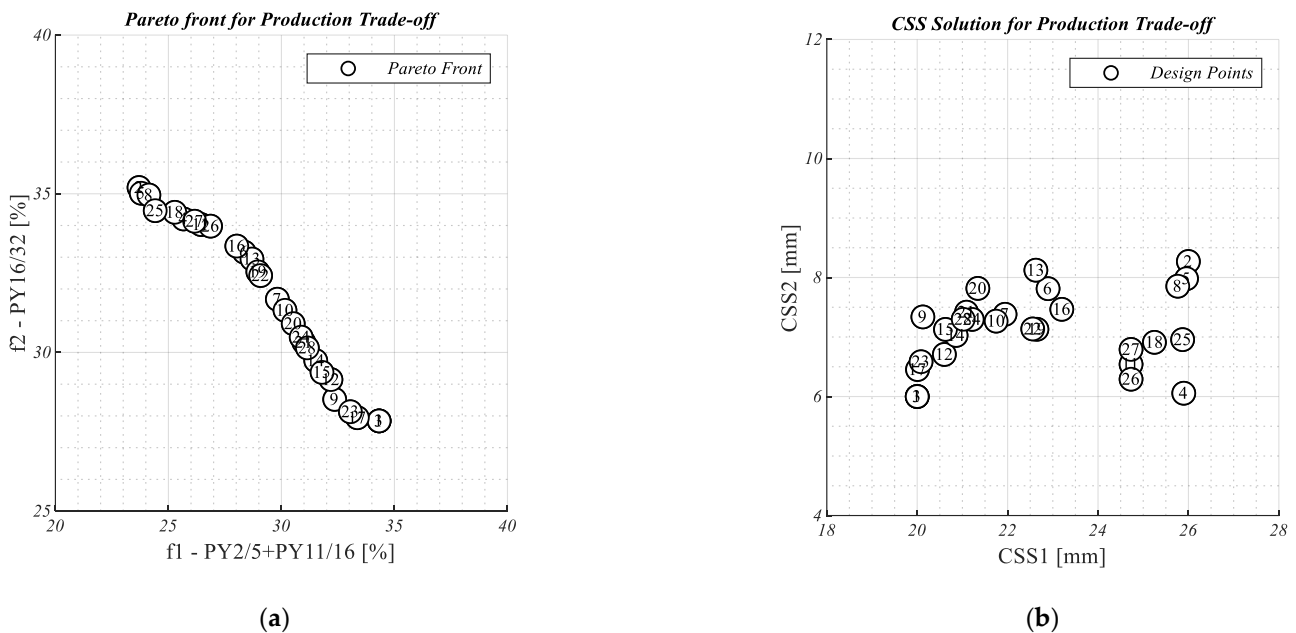


Figure 14. (a) Trade-off curve and (b) solution points of the optimization problem in Equation (15), when P8/11 is recirculated.

Case 6: The trade-off curves are generated for an operational scenario where the product P5/8 is recirculated for re-crushing as per Equation (16). Figure 15a shows the values for the objective to maximize the production of P2/5 and P8/11 while minimizing the production of coarser products P11/16 and P16/32. Here, the solution space is interior optima for both CSS1 and CSS2 as shown in Figure 15b. This example shows that the proportion of improvements can be achieved by adjusting both variables simultaneously.

$$\begin{aligned}
 &\min f_1 = P2/5_{TR} + P11/16_{TR}, f_2 = P11/16_{TR} + P16/32_{TR} \\
 &w.r.t \rightarrow CSS_1, CSS_2 \\
 &s.t. \\
 &20 \leq CSS_1 \leq 26 \\
 &6 \leq CSS_2 \leq 10 \\
 &where, f_1 \text{ and } f_2 \text{ is expressed as } [t/h]
 \end{aligned}
 \tag{16}$$

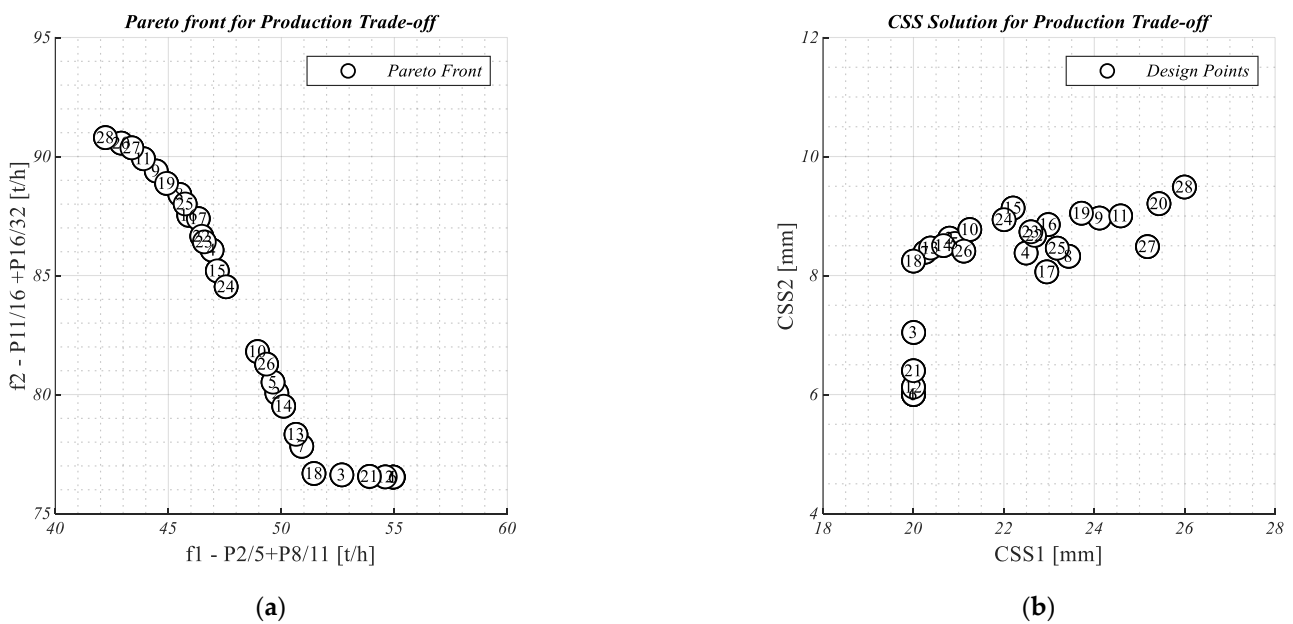


Figure 15. (a) Trade-off curve and (b) solution points of the optimization problem in Equation (16), when P5/8 is recirculated.

Case 7: In most aggregates’ operations, there are issues with excessive fines. The trade-off curves are generated for an operational scenario where the product P5/8 is recirculated for re-crushing. Figure 16a shows the values for the objective to maximize the product yield of P2/5 while minimizing the yield of the sum of remaining products, see Equation (17). For the application of one product vs. others, the trade-off of the yield is linear in nature. Although the solution points are interesting as there are multiple solutions available for similar performance levels, for example, solution numbers 27, 5 and 15.

$$\begin{aligned}
 \min f_1 &= PY2/5_{TR}, f_2 = PY0/2_{TR} + PY8/11_{TR} + PY11/16_{TR} + PY16/32_{TR} + PY32/64_{TR} \\
 w.r.t &\rightarrow CSS_1, CSS_2 \\
 s.t. & \\
 20 &\leq CSS_1 \leq 26 \\
 6 &\leq CSS_2 \leq 10 \\
 \text{where, } f_1 \text{ and } f_2 &\text{ is expressed as [\%]}
 \end{aligned}
 \tag{17}$$

Case 8: The trade-off curves are generated for an operational scenario where the product P8/11 is recirculated for re-crushing and the objective is to maximize two product yields P2/5 and P5/8 against the rest of the product yields. Figure 17a shows the values for the objective functions and Figure 17b shows the solution points for the optimization problem posed in Equation (18). Again, the trade-off curve is linear while the solution points are scattered with multiple solutions at similar performance levels.

$$\begin{aligned}
 \min f_1 &= PY2/5_{TR} + PY5/8_{TR}, f_2 = PY0/2_{TR} + PY11/16_{TR} + PY16/32_{TR} + PY32/64_{TR} \\
 w.r.t &\rightarrow CSS_1, CSS_2 \\
 s.t. & \\
 20 &\leq CSS_1 \leq 26 \\
 6 &\leq CSS_2 \leq 10 \\
 \text{where, } f_1 \text{ and } f_2 &\text{ is expressed as [\%]}
 \end{aligned}
 \tag{18}$$

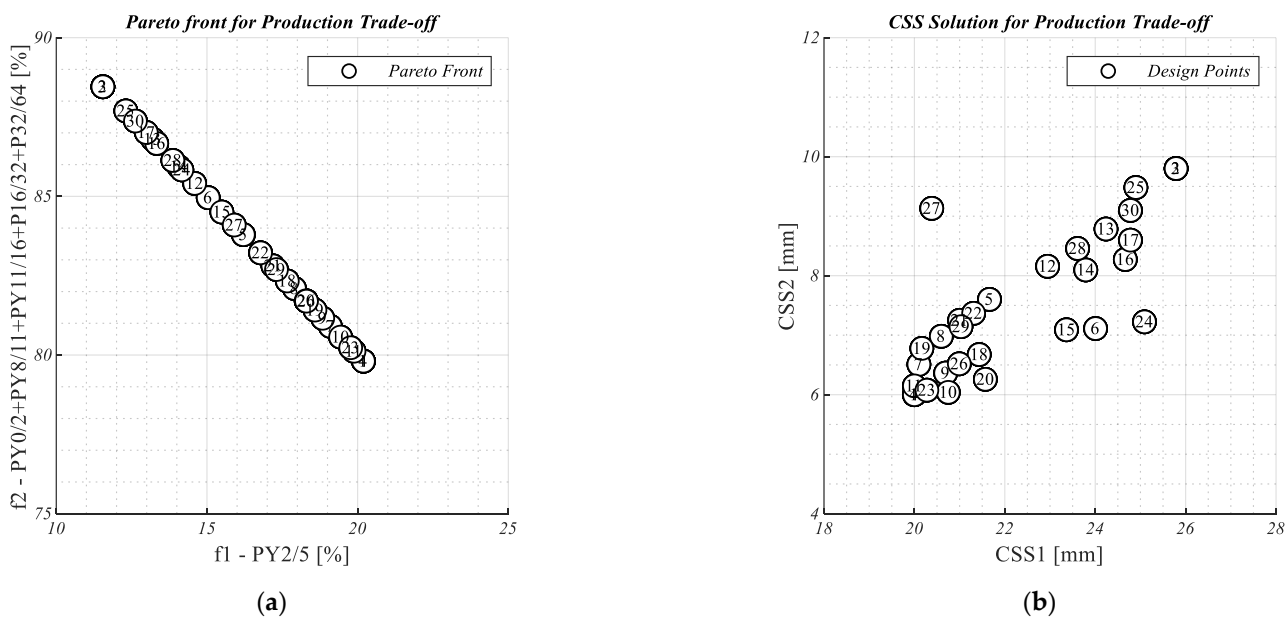


Figure 16. (a) Trade-off curve and (b) solution points of the optimization problem in Equation (17), when P5/8 is recirculated.

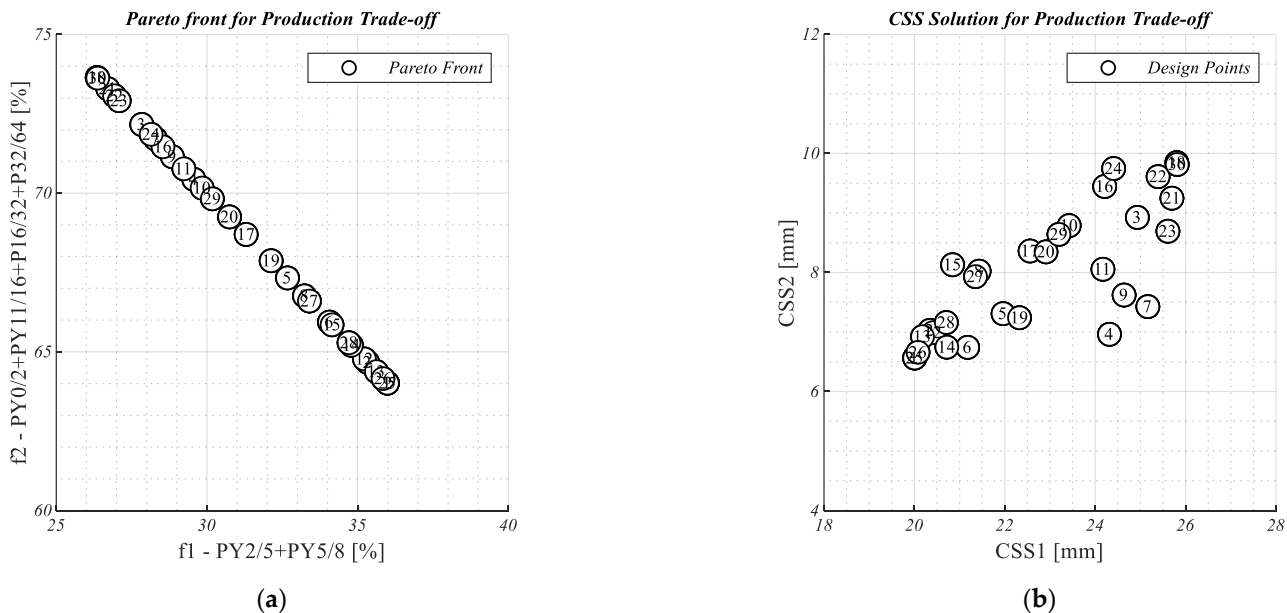


Figure 17. (a) Trade-off curve and (b) solution points of the optimization problem in Equation (18), when P8/11 is recirculated.

5. Discussion and Conclusions

The paper presented systematic implementation optimization functionality for crushing plants. The use of unconstrained gradient-based optimization (Quasi-Newton method) approach for crusher model calibration together with the configuration of dynamic process simulation provided a reliable response for crushing plant operation. The model captured the response of multiple feed changes to the crusher. The dynamic process simulation showed the effect of variable bin filling rate and production change as the two crusher settings were changed simultaneously. The response of the simulation is closer to practical industrial operations.

The operation of complex aggregate plants holds flexibility in production operations. The use of multi-objective optimization using a non-gradient algorithm (genetic algorithm)

provided opportunities to explore the solution space depending on the operational objectives. Multiple cases of trade-off curves (Pareto Front) were demonstrated to provide the quantification of the production flexibility together with the solution points. The solution space largely varied as the objectives and scenario of the operation changed. The solution space for each case can be further restricted if constraints are added to the optimization problem.

The choice of objective function used for a trade-off analysis is dependent on the situational requirements of operations. Product quantity can be useful to meet the direct demands of the customer, although it is dependent on the operational scenario. The product throughput can be useful to steer the production rate of different products. The product yield is more useful in a scenario for increasing/decreasing the proportion of production when there is a sufficient stockpile of products present. All the objectives provide the quantification of flexibility present for the solution space of an operational setting.

The solution space (CSS solutions) for different optimization cases is dependent on the topology of the plant. In the presented results, the sensitivity of the crusher CC1 was higher on the products as compared to the crusher CC2. As the objective function was based on product throughput, the solution space was largely governed by the crusher CC1 and was decoupled to crusher CC2. When the objective was product yield, both the CSS were active simultaneously for the two crushers. As the plant topology changes, the results obtained can be different as the design freedom will change.

The trade-off curves can be useful for plant managers and operators of the crushing plant to make daily decisions regarding production. The application of trade-off curves can be extended to connect the market demands to daily operational choices. The trade-off curves using other objectives such as specific energy can be studied in future works. The use of trade-off curves can be extended to the design stage of the crushing plant for greenfield projects, as the flexibility of the new plant design can be quantified easily. This can enable enhanced knowledge of the plant's performance at the design stage.

Author Contributions: Conceptualization, K.B., G.A. and E.H.; methodology, K.B. and G.A.; software, K.B. and G.A.; validation, K.B. and G.A.; formal analysis, K.B. and G.A.; investigation, K.B., G.A. and E.H.; resources, E.H. and M.S.A.; data curation, K.B.; writing—original draft preparation, K.B.; writing—review and editing, K.B., G.A., E.H., M.E. and M.S.A.; visualization, K.B.; supervision, G.A., E.H. and M.E.; project administration, K.B. and E.H.; funding acquisition, E.H. and M.S.A. All authors have read and agreed to the published version of the manuscript.

Funding: This research was funded by Svenska Byggbranschens Utvecklingsfond (SBUF), Project Number: 13753 (Development Fund of the Swedish Construction Industry).

Data Availability Statement: Restrictions apply to the availability of these data. Data were obtained from Swerock AB and are available from the authors with the permission of Swerock AB.

Acknowledgments: This work has been performed under the project: "Optimering av verkliga processer för bergmaterialproduktion" and supported financially by "Svenska Byggbranschens Utvecklingsfond"—SBUF, Project Number: 13753 (Development Fund of the Swedish Construction Industry). Swerock AB and its personnel in Källered Bergtäkt, Mölndal, Sweden are gratefully acknowledged for all their support and efforts to make this work possible. This work has been performed within the Sustainable Production Initiative and the Production Area of Advance at Chalmers; this support is gratefully acknowledged.

Conflicts of Interest: The authors declare no conflict of interest. The funders had no role in the design of the study; in the collection, analyses or interpretation of data; in the writing of the manuscript; or in the decision to publish the results.

References

1. SS-EN 13450/AC:2012; Aggregates for Railway Ballast. Swedish Institute of Standards: Stockholm, Sweden, 2012.
2. SS-EN 13043/AC:2006; Aggregates for Bituminous Mixtures and Surface Treatments for Roads, Airfields and Other Trafficked Areas. Swedish Institute of Standards: Stockholm, Sweden, 2006.
3. Asbjörnsson, G. Crushing Plant Dynamics. Ph.D. Thesis, Chalmers University of Technology, Gothenburg, Sweden, 2015.
4. Yamashita, A.S.; Thivierge, A.; Euzébio, T.A.M. A review of modeling and control strategies for cone crushers in the mineral processing and quarrying industries. *Miner. Eng.* **2021**, *170*, 107036. [[CrossRef](#)]
5. Bhadani, K. Optimization Capabilities for Crushing Plants. Ph.D. Thesis, Chalmers University of Technology, Gothenburg, Sweden, 2022.
6. King, R.P. *Modeling and Simulation of Mineral Processing Systems*; Elsevier Science: Amsterdam, The Netherlands, 2001.
7. Napier-Munn, T.J.; Morrell, S.; Morrison, R.D.; Kojovic, T. *Mineral Comminution Circuits: Their Operation and Optimisation*; Julius Kruttschnitt Mineral Research Centre, The University of Queensland: Indooroopilly, QLD, Australia, 1996.
8. Evertsson, C.M. Cone Crusher Performance. Ph.D. Thesis, Chalmers University of Technology, Gothenburg, Sweden, 2000.
9. Soldinger, M. Screening of crushed rock material. Ph.D. Thesis, Chalmers University of Technology, Gothenburg, Sweden, 2002.
10. Karra, V.K. Development of a model for predicting the screening performance of a vibrating screen. *CIM Bull.* **1979**, *72*, 167–171.
11. Whiten, W.J. The simulation of crushing plants with models developed using multiple spline regression. *J. S. Afr. Inst. Min. Metall.* **1972**, *72*, 257–264.
12. Whiten, W.J. Models and control techniques for crushing plants. In Proceedings of the Mineral/Metallurgical Processing (1st International Symposium on Automatic Control in Mineral Processing and Process Metallurgy), Los Angeles, CA, USA, 27 February–1 March 1984; pp. 217–225.
13. King, R.P. Simulation—The modern cost-effective way to solve crusher circuit processing problems. *Int. J. Miner. Process.* **1990**, *29*, 249–265. [[CrossRef](#)]
14. Bhadani, K.; Asbjörnsson, G.; Schnitzer, B.; Quist, J.; Hansson, C.; Hulthén, E.; Evertsson, M. Applied Calibration and Validation Method of Dynamic Process Simulation for Crushing Plants. *Minerals* **2021**, *11*, 921. [[CrossRef](#)]
15. Bhadani, K.; Asbjörnsson, G.; Hulthén, E.; Evertsson, C.M. Development and implementation of key performance indicators for aggregate production using dynamic simulation. *Miner. Eng.* **2020**, *145*, 106065. [[CrossRef](#)]
16. Muller, D.; de Villiers, P.G.R.; Humphries, G. A Holistic Approach to Control and Optimisation of an Industrial Crushing Circuit. *IFAC Proc. Vol.* **2010**, *43*, 142–146. [[CrossRef](#)]
17. Bhadani, K.; Asbjörnsson, G.; Hulthén, E.; Evertsson, C.M. Application of multi-disciplinary optimization architectures in mineral processing simulations. *Miner. Eng.* **2018**, *128*, 27–35. [[CrossRef](#)]
18. Duarte, R.A.; Yamashita, A.S.; da Silva, M.T.; Cota, L.P.; Euzébio, T.A.M. Calibration and Validation of a Cone Crusher Model with Industrial Data. *Minerals* **2021**, *11*, 1256. [[CrossRef](#)]
19. While, L.; Barone, L.; Hingston, P.; Huband, S.; Tuppurainen, D.; Bearman, R. A multi-objective evolutionary algorithm approach for crusher optimisation and flowsheet design. *Miner. Eng.* **2004**, *17*, 1063–1074. [[CrossRef](#)]
20. Huband, S.; Barone, L.; Hingston, P.; While, L.; Tuppurainen, D.; Bearman, R. Designing comminution circuits with a multi-objective evolutionary algorithm. In Proceedings of the 2005 IEEE Congress on Evolutionary Computation, Edinburgh, UK, 2–5 September 2005; pp. 1815–1822.
21. Huband, S.; Tuppurainen, D.; While, L.; Barone, L.; Hingston, P.; Bearman, R. Maximising overall value in plant design. *Miner. Eng.* **2006**, *19*, 1470–1478. [[CrossRef](#)]
22. Sbárbaro, D.; del Villar, R. *Advanced Control and Supervision of Mineral Processing Plants*; Springer: London, UK, 2010; pp. 1–14. [[CrossRef](#)]
23. Jacob, K.V.; Mehos, G.; Carson, J.W.; Fan, Y.; Freireich, B.J.; Koch, J.F.; Dhodapkar, S.V.; Jain, P. Modeling and simulation of grinding processes. In *Perry's Chemical Engineers' Handbook*, 9th ed.; Green, D.W., Southard, M.Z., Eds.; McGraw-Hill Education: New York, NY, USA, 2019.
24. Asbjörnsson, G.; Hulthén, E.; Evertsson, C.M. Modelling and simulation of dynamic crushing plant behavior with MATLAB/Simulink. *Miner. Eng.* **2013**, *43*, 112–120. [[CrossRef](#)]
25. Bond, F.C. Third theory of comminution. *Min. Eng.* **1952**, *4*, 484.
26. Asbjörnsson, G.; Hulthén, E.; Evertsson, C.M. Modelling dynamic behaviour of storage bins for material handling in dynamic simulations. In Proceedings of the XXVI International Mineral Processing Congress, New Delhi, India, 24–28 September 2012; pp. 258–267.
27. SS-EN 933-1:2012; Tests for Geometrical Properties of Aggregates—Part 1: Determination of Particle Size Distribution—Sieving Method. Swedish Standards Institute: Stockholm, Sweden, 2012.
28. Fletcher, R. *Practical Methods of Optimization*; John Wiley & Sons, Incorporated: New York, NY, USA, 2000.
29. Kalyanmoy, D. *Multi-Objective Optimization Using Evolutionary Algorithms*; John Wiley & Sons, Inc.: Hoboken, NJ, USA, 2001.
30. Bhadani, K.; Asbjörnsson, G.; Hulthén, E.; Bengtsson, M.; Evertsson, M. Comparative Study of Optimization Schemes in Mineral Processing Simulations. In Proceedings of the XXIX International Mineral Processing Congress, Moscow, Russia, 17–21 September 2018.

31. Belegundu, A.D.; Chandrupatla, T.R. *Optimization Concepts and Applications in Engineering*; Cambridge University Press: Cambridge, UK, 2011.
32. Kramer, O. Genetic Algorithms. In *Genetic Algorithm Essentials*; Springer International Publishing: Cham, Switzerland, 2017; pp. 11–19. [[CrossRef](#)]

Disclaimer/Publisher’s Note: The statements, opinions and data contained in all publications are solely those of the individual author(s) and contributor(s) and not of MDPI and/or the editor(s). MDPI and/or the editor(s) disclaim responsibility for any injury to people or property resulting from any ideas, methods, instructions or products referred to in the content.